International Journal of Engineering and Technology Innovation, vol. 7, no. 3, 2017, pp. 201 - 216

Comparative Study on Photovoltaic Pumping Systems Driven by Different Motors Optimized with Sliding Mode Control

Abdelhak Bouchakour[1,*], Mostéfa Brahami[1] and Abdelhalim Borni[2]

[1]Intelligent Control and Electrical Power Systems, Djillali Liabes, University of Sidi Bel Abbes, Algeria.

[2] Applied Research Unit for Renewable Energies, URAER, Renewable Energy Development Center, Algeria.

Received 16 October 2016; received in revised form 26 January 2017; accepted 31 January 2017

Abstract

This study investigates the performance of three different photovoltaic (PV) water pumping systems driven by three types of motors, namely a separately excited DC motor (DCM), an asynchronous motor (ASM), and a permanent magnet synchronous motor (PMSM), via a DC/DC buck-boost converter coupled to a centrifugal pump. The purpose of this study is to implement a fast and robust control for this type of a nonlinear system, controlled by sliding mode (SM). This paper presents an SM control technique for controlling a DC/DC buck-boost converter to transfer the maximum power delivered by the PV generator. Each component is studied and analyzed to simulate the global system in MATLAB/SIMULINK. The three systems are then compared to determine the overall effectiveness of the proposed command. The study concludes that the ASM-driven PV system yields highly favorable results and requires less maintenance compared with other systems.

Keywords: photovoltaic generator, buck-boost converter, permanent magnet synchronous motor, centrifugal pump

Nomenclature

I	Generator current	[A]	i_{sd}	d-axis stator current	[A]
I_{pv}	Photocurrent	[A]	i_{sq}	q-axis stator current	[A]
I_0	Inverse saturation current	[A]	J_m	Moment of inertia	[kg/m^2]
R_s, R_{sh}	Series and parallel resistance respectively	[Ω]	K_E	Motor speed constant	
I_d	Diode current	[A]	K_T	Motor torque constant	
A	Quality factor of the diode		L_a	Armature inductance	[H]
K	Boltzmann's constant	[J/K]	L_d	d-axis self-inductance of the stator	[H]
q	Electronic charge	[C]	L_q	q-axis self-inductance of the stator	[H]
e_a	Applied voltage	[V]	L_r	Rotor self-inductance	[H]
R_a	Armature resistance	[Ω]	L_s	Stator self-inductance	[H]
i_a	Motor armature current	[A]	M	Mutual inductance	[H]
E	Motor electromotive	[V]	P	Number of pole pairs	[H]
φ_f	Rotor flux	[Web]	P_n	Motor output rated power	[W]
$\theta_{e,m}$	Electrical and mechanical angle	[rad]	Q	Water discharge rate	[m^3/h]
f	Friction coefficient		T_e	Electromagnetic developed torque	[N.m]
B_m	Viscose friction coefficient	[Nm/(rad/s)]	T_P	Pump torque	[N.m]
v_{sd}	d-axis stator voltage	[V]	H	Total head	[m]
n_p	Pump efficiency		ρ	Water volumic masse	[kg/m^3]
P_p	Pump power	[W]	n_m	Motor efficiency	
P_c	Output power of the converter	[W]	n_c	Converter efficiency	

* Corresponding author. E-mail: abdelhak.bouchakour@yahoo.fr

1. Introduction

Several studies have focused on the development of clean renewable energy sources [1]. Many forms of renewable energy, such as wind, solar, hydro, biomass, and geothermal energy, can contribute to reducing the greenhouse effect [2].

Solar energy is a free [3], clean, and inexhaustible resource that can be used in various applications [4]. The electricity supplied by the national electric grid may not reach some remote areas. Therefore, solar energy is particularly critical in developing countries, where solar energy can be used for lighting as well as irrigation and pumping water [5].

Therefore, different types of motors, such as DC motors (DCMs), permanent magnet synchronous motors (PMSMs), and induction motors (IMs), are used in water pumping systems [6]; each motor has unique characteristics that determine its effectiveness [7].

However, AC motors require a DC/AC inverter to be installed between the solar panels and the motor [8]. Compared with other motors, a DCM is considered the first choice for pumping water because it can be easily controlled owing to the natural decoupling of flux and torque [9]. However, studies on numerous direct coupling DCMs have reported maintenance problems on these motors [10]. Moreover, commutator arcing problems limit the size and speed of these motors, making them unsuitable [11].

These limitations can be overcome by using PV pumping systems driven by a PMSM with or without a DC/DC converter because of their wide range of input voltages [12]. However, these systems are expensive and applicable at only low power, thus hampering their utility [13]. Contrastingly, because of their easy availability, high efficiency, low maintenance, low cost, durable design, and small size, IM-based water pumping systems have attracted considerable interest from researchers and manufacturers [14].

Over the past years, PV system optimization has attracted considerable attention. Consequently, many algorithms, such as perturbation and observation (P&O) and incremental conductance (INC) algorithms, fractional open circuit voltage, neural networks, and fuzzy control, have been developed for tracking the maximum power of PV generators (PVGs), optimizing motor efficiency, and maximizing global efficiency [15]. These algorithms differ with regard to simplicity, effectiveness, convergence speed, complexity, dynamic performance under rapidly changing climate conditions, and cost [16].

In this work, to study and compare the operating performance of the PV pumping systems, a command based on the sliding mode (SM) was developed and implemented in three types of PV pumping systems driven by an ASM, PMSM, and DCM by using the same power. This paper first introduces a PV cell model. Then, a model of a buck-boost converter for maximizing PVG power is presented, followed by electrical motor modeling with a vectorial command. Next, the design of the SM control is discussed. Finally, the conclusion summarizes the main points.

2. PV Water Pumping System Analysis

The studied *PV* water pumping system consists of three components: the *PV* array, the converters (*DC/DC or DC/AC*), and the moto-pump. Each element has its own characteristics. Fig. 1 shows the overall structure of the system.

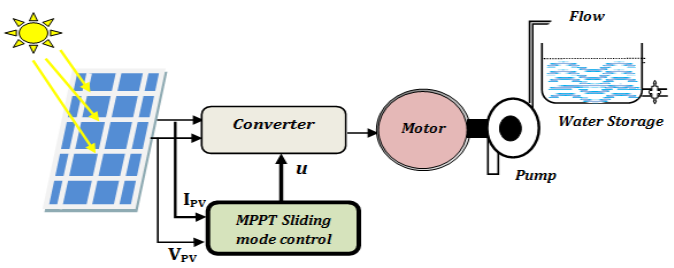

Fig. 1 *PV* Water pumping system used in this study

2.1. Modeling of PVG

A PVG comprises several cells connected to each other, in parallel and in series, to provide the desired voltage and output current [17]. Fig. 2 shows the electrical circuit of a PV cell.

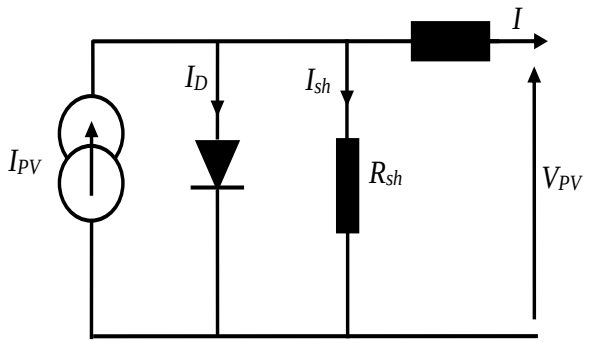

Fig. 2 Electrical circuit of the PV cell

This model represents the solar cell as a current source arranged in parallel to a diode. The resistance connected in series is the contact resistance, whereas the one connected in parallel is the shunt resistance representing leakage currents [6].The characteristic equation of the solar cell output current I is given by [16].

$$I = I_{PV} - I_0(exp\frac{V_{PV} + R_S I}{A} - 1) - \frac{V_{PV} + R_S I}{R_{sh}} \quad (1)$$

The output characteristics of the *PV* array are nonlinear and critically affected by solar radiation, temperature, and load conditions. To maximize its output power, the PV array should be operated at a unique point with a specific voltage and current or at a specific load resistance [18]. When a resistive load is powered by the PV array, the operating point may be far from the maximum power point (MPP), according to the insolation and temperature values (Fig. 3).

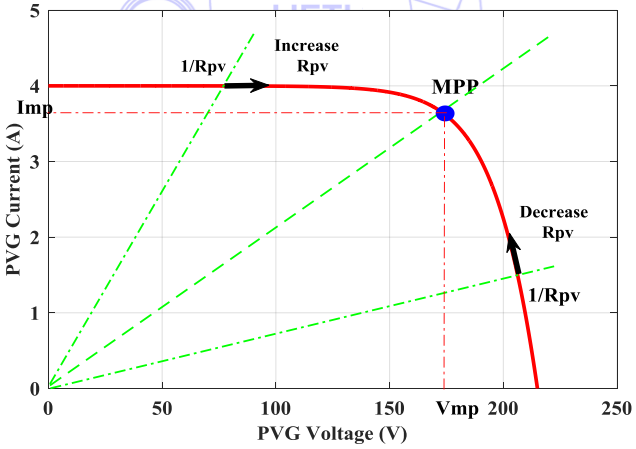

Fig. 3 *IV* characteristics of the *PV* panel

For maintaining the *PV* module at the *MPP*, an *MPP* tracking controller based on the *SM* is used to control the switched mode *DC/DC* converter for load matching [19].

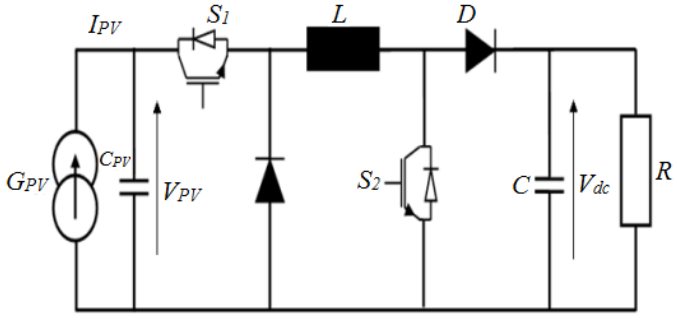

Fig. 4 Simplified diagram of a buck-boost converter

$$\begin{cases} \dfrac{dV_{pv}}{dt} = \dfrac{i_{pv}}{C_{pv}} - \dfrac{i_L}{C_{pv}} \\ L\dfrac{di_L}{dt} = uV_{pv} - (1\text{-}u)V_{dc} \\ C\dfrac{dV_{dc}}{dt} = (1-u)i_L - \dfrac{V_{dc}}{R} \end{cases} \tag{2}$$

where u is the duty cycle, which defines the switch position. The objective is to regulate the output voltage V_{dc} around the desired voltage [16].

3. Electrical Motor Modeling

3.1. DCM model

When using small loads, DCMs are preferable because they are simple to use and effective [20]. DCMs are highly economical because a PVG supplies DC, thereby eliminating the need for a DC/AC inverter [21]. The characteristic equation of a DCM can be expressed as [22].

$$e_a = i_a R_a + L_a \frac{di_a}{dt} + E \tag{3}$$

The electromotive E (*e.m.f*) can be expressed by

$$E = K_E \omega_m \tag{4}$$

The electromagnetic torque is related to the armature current by

$$T_e = K_T i_a \tag{5}$$

3.2. PMSM model

The following characteristic equation of a *PMSM* can be expressed as [23]

$$\begin{bmatrix} v_d \\ v_q \end{bmatrix} = \begin{bmatrix} R_s + pL_d & -P\omega_m L_q \\ P\omega_m L_d & R_s + pL_q \end{bmatrix} \begin{bmatrix} i_d \\ i_q \end{bmatrix} + \begin{bmatrix} 0 \\ P\omega_m \varphi_f \end{bmatrix} \tag{6}$$

$$T_e = P\left[\left(L_d - L_q\right) i_d + \varphi_f\right] i_q \tag{7}$$

For a synchronous machine with smooth poles ($L_d = L_q$), the torque is $T_e = P\varphi_f i_q$.The mechanical equation of a *PMSM* is expressed by

$$J\frac{d\omega}{dt} + f\omega = T_e - T_r \tag{8}$$

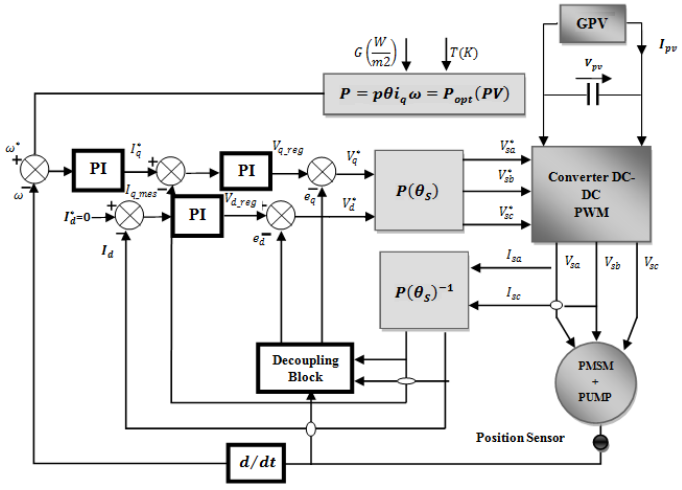

Fig. 5 Representative schema of the vectorial command of *PMSM*

Fig. 5 represents the vector control of a *PMSM* in a coordinate (*dq*) system. The matrix shows that v_d and v_q depend on the stator currents, and hence the need for implementing a decoupling. Coupling is eliminated using the compensation method. The control currents are set by neglecting the coupling terms added to the current regulator outputs to obtain reference voltages [24].The terms of reference are then expressed by

$$\begin{cases} e_d = -\omega L_d i_q \\ e_q = \omega (L_d i_d + \varphi_f) \end{cases} \tag{9}$$

$$\begin{cases} V_d^* = (R + sL_d) i_d - \omega L_d i_q \\ V_q^* = (R + sL_q) i_q + \omega (L_d i_d + \varphi_f) \end{cases} \tag{10}$$

$$\begin{cases} V_d^* = V_{d\_reg} - e_d \\ V_q^* = V_{q\_reg} - e_q \end{cases} \tag{11}$$

The closed loop transfer functions of a PMSM are represented by the following equations.

$$\begin{cases} F_d(s) = \dfrac{I_d(s)}{V_{d\_reg}(s)} = \dfrac{1}{R_S + s.L_d} \\ F_q(s) = \dfrac{I_q(s)}{V_{q\_reg}(s)} = \dfrac{1}{R_S + s.L_q} \end{cases} \tag{12}$$

The reference of *DC* I_d* is set to zero. The inverter output voltage is controlled using a pulse-width modulation technique (*PWM*), which enables the simultaneous adjustment of the frequency and output voltage [21].

3.3. IM model

The characteristic equation of the *IM* in the coordinate (*dq*) axis [25] can be expressed as

$$\begin{bmatrix} v_{sd} \\ v_{sq} \\ 0 \\ 0 \end{bmatrix} = \begin{bmatrix} (R_s + \frac{M^2}{L_r T_r} + p\sigma L_s) & -\sigma L_s \omega_s & -\frac{M}{L_r T_r} & -\frac{M}{L_r} P\omega_m \\ \sigma L_s \omega_s & (R_s + \frac{M^2}{L_r T_r} + p\sigma L_s) & \frac{M}{L_r} P\omega_m & -\frac{M}{L_r T_r} \\ -\frac{M}{T_r} & 0 & (p + \frac{1}{T_r}) & -(\omega_s - P\omega_m) \\ 0 & -\frac{M}{L_r T_r} & (\omega_s - P\omega_m) & (p + \frac{1}{T_r}) \end{bmatrix} \begin{bmatrix} i_{sd} \\ i_{sq} \\ \varphi_{rd} \\ \varphi_{rq} \end{bmatrix} \tag{13}$$

$$T_e = P \frac{M}{L_r} (\varphi_{rd} i_{sq} - \varphi_{rq} i_{sd}) \tag{14}$$

$$J \frac{d\omega}{dt} + f\omega = T_e - T_r \tag{15}$$

where $T_r = \frac{L_r}{r_r}$ is the rotor time constant, $\sigma = 1 - (M^2 / L_s L_r)$ is the dispersion coefficient.

Fig. 6 shows the vectorial command of the IM in the coordinate (*dq*) system used for regulating the current and flux according to their reference values. The key feature of this control technology is the presence of a natural decoupling between the rotor flux and electromagnetic torque. Decoupling is achieved by controlling both components of the stator current vectors i_{sd} and i_{sq}. The electromagnetic torque is then given by

$$T_e = P \frac{M}{L_r} (\varphi_{rd} i_{sq}) \tag{16}$$

According to Eq. (16), rotor flux depends on the component i_{sd}, whereas electromagnetic torque depends on the component i_{sq}. The transfer functions in the closed loop of the current regulator, and flux controller are given by

$$\frac{i_{ds}}{v_{sd}} = \frac{1}{R_s + \sigma L_s s} \tag{17}$$

$$\frac{i_{qs}}{v_{sq}} = \frac{1}{R_s + \sigma L_s s} \tag{18}$$

$$\frac{\varphi_{dr}}{i_{ds}} = \frac{M}{1 + \tau_r s} \tag{19}$$

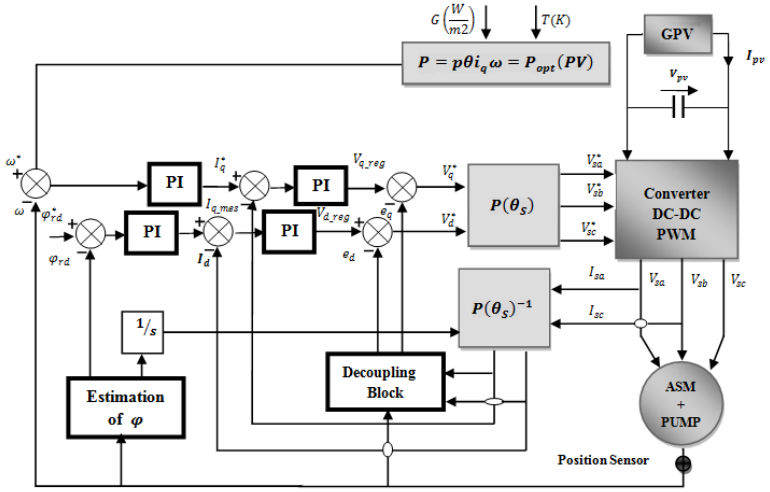

Fig. 6 Representative schema of the vectorial command of *IM*

4. Determination of the Reference Speed Motors

$$\begin{cases} P_p = K_p.\omega^3 \\ P_{mec} = \dfrac{P_p}{n_p} \end{cases} \tag{20}$$

The motor power [26] can also be determined as

$$P_m = n_m.P_c \tag{21}$$

The optimal speed of the *PVG* is given by

$$\omega_{ref} = \sqrt[3]{\frac{n_h.n_c.n_m.n_p.I_{max}.V_{max}}{K_p}} \tag{22}$$

5. Model of the PWM Inverter

A *DC/AC* inverter is included between the *PVG* and the pump for the systems driven by the *PMSM* or *IM* [18].

$$\begin{cases} V_{an} = V_{ao} - V_{no} \\ V_{bn} = V_{bo} - V_{no} \\ V_{cn} = V_{co} - V_{no} \end{cases} \tag{23}$$

The representative equation is expressed as

$$V_{an} + V_{bn} + V_{cn} = 0 \tag{24}$$

Also,

$$V_{ao} + V_{bo} + V_{co} = 3V_{no} \tag{25}$$

Thus, the output phase voltages will be

$$\begin{bmatrix} V_{an} \\ V_{bn} \\ V_{cn} \end{bmatrix} = \frac{1}{3}\begin{bmatrix} 2 & -1 & -1 \\ -1 & 2 & -1 \\ -1 & -1 & 2 \end{bmatrix}\begin{bmatrix} V_{pv} \end{bmatrix} \tag{26}$$

6. Centrifugal Pump Model

The operating parameters for a centrifugal pump are the pumping head (H), pump capacity (Q), and shaft power (T), which are functions of the impeller speed (ω_m). The $H(Q)$ characteristic can be determined by [24].

$$H = a_0\omega_m^2 - a_1\omega_m Q - a_2 Q^2 \tag{27}$$

where a_0, a_1 and a_2 are constant parameters given by the manufacturer.

$$T_L = k_r\omega_m^2 \tag{28}$$

$$H = H_g + \Delta H \tag{29}$$

ΔH depends on driving and friction losses of the pipe, it is given by

$$\Delta H = (\lambda\frac{l}{d} + \varepsilon)\frac{8Q^2}{\pi^2 d^4 g} \tag{30}$$

The hydraulic power is given by:

$$P_H = \rho g Q H \tag{31}$$

7. SM Control Design

The easy implementation and robustness of the *SM* control with regard to system uncertainties and external disturbances has considerably increased its popularity. The robustness of this mode is characterized by the possibility of selecting a function and switching logic. Thus, the design of the *SM* controller has two steps: the definition of the adequate switching surface S (.) and the development of the switching logic U. The system state converges to a definite area, producing a zigzag motion in a band near the switching surface. This band is the real seat of the *SM* and is called the pseudo *SM* [2].

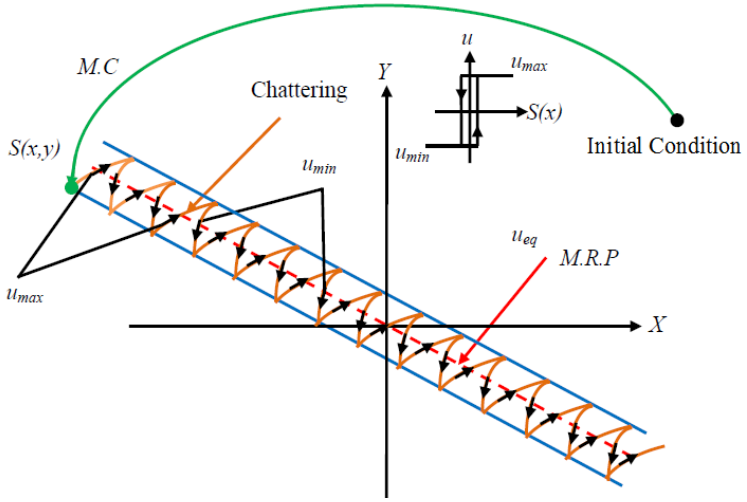

Fig. 7 Real sliding mode

These conditions can be defined by the direct switching function or Lyapunov stability function to force the system's trajectory toward the sliding surface. The selected Lyapunov function is greater than zero and decreasing. To achieve this, the variable x should tend toward its reference, which is ensured by the control V [27].

When the generator produces a maximum power, the sliding surface is zero:

$$V(x) = \frac{1}{2} S^2(x) \tag{32}$$

$$\dot{V}(x) = S(x).\dot{S}(x) \tag{33}$$

The control U equals to:

$$U = U_{eq} + U_n \tag{34}$$

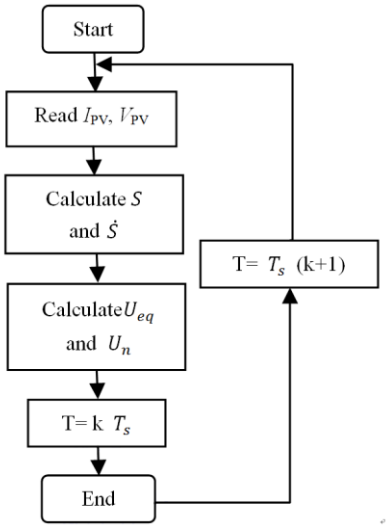

Fig. 8 Flowchart of sliding mode control

The sliding surface is defined by $S = \frac{\partial P_{pv}}{\partial V_{pv}}$, and the sliding surface is zero when the generator provides maximum power, i.e.,

$$S = \frac{\partial P_{pv}}{\partial V_{pv}} = \frac{\partial (i_{pv}.V_{pv})}{\partial V_{pv}} = 0 \tag{35}$$

$$\frac{\partial P_{pv}}{\partial V_{pv}} = \frac{\partial i_{pv}}{\partial V_{pv}} V_{pv} + i_{pv} = 0 \tag{36}$$

The switch control signal is defined according to the sign of the sliding surface and they can be selected as

$$Un = \begin{cases} 0 & S \geq 0 \\ 1 & S < 0 \end{cases} \tag{37}$$

The derivative of the surface is given by

$$S(x) = \frac{\partial S}{\partial x^T} f(x) \tag{38}$$

$$\dot{S}(x) = -\frac{\partial S}{\partial x^T} \dot{x} = \frac{\partial S}{\partial x^T} f(x) + \frac{\partial S}{\partial x^T} g(x) U_{eq} \tag{39}$$

To define the command U_{eq}, the derivative of the surface equal to zero $\dot{S}(x) = 0$

$$U_{eq} = -\frac{\frac{\partial S}{\partial x^T} f(x)}{\frac{\partial S}{\partial x^T} g(x)} = -\frac{L_f S(x)}{L_g S(x)} \tag{40}$$

$$L_f h_2 = \frac{\partial h_2}{\partial x^T} f(x) = \left(\frac{\partial^2 i_{pv}}{\partial^2 V_{pv}} V_{pv} + 2\frac{\partial i_{pv}}{\partial V_{pv}}\right)\frac{i_{pv}}{C} \tag{41}$$

$$L_g h_2 = \frac{\partial h_2}{\partial x^T} g(x) = \left(\frac{\partial^2 i_{pv}}{\partial^2 V_{pv}} V_{pv} + 2\frac{\partial i_{pv}}{\partial V_{pv}}\right)\left(-\frac{i_L}{C}\right) \tag{42}$$

By substituting Eqs. (41) and (42) into Eq. (40), the equivalent control variable can be expressed as

$$U_{eq} = \frac{i_{pv}}{i_L} \tag{43}$$

The equation of the system Eq. (36) can be written as

$$\dot{x} = f(X) + g(X)u \tag{44}$$

where

$$\dot{x} = \begin{bmatrix} \dot{V}_{pv} \\ \frac{\partial i_L}{\partial t} \\ \dot{V} \end{bmatrix} \quad f(x) = \begin{bmatrix} \frac{i_{pv}}{C_{pv}} \\ \frac{V}{L} \\ -\frac{i_L}{C} - \frac{V}{RC} \end{bmatrix} \quad g(x) = \begin{bmatrix} -\frac{i_L}{C_{pv}} \\ \frac{V_{pv} - V}{L} \\ \frac{i_L}{C} \end{bmatrix}$$

By substituting (43) in (34), the final model is given by

$$U = -\frac{i_{pv}}{i_L} + K_u sgn(S(i_{pv})) \tag{45}$$

5.1. Convergence and living conditions

The Lyapunov stability function is one of the methods used to study the stability and convergence of the sliding surface [27].

$$V(X) = \frac{1}{2} S^2(X) > 0 \tag{46}$$

The derivative is

$$\dot{V}(X) = S\frac{dS}{dt} = \frac{\partial P_{PV}}{\partial t}\frac{d}{dt}\left(\frac{\partial P_{PV}}{\partial V_{PV}}\right) \tag{47}$$

By substituting Eq. (1) in Eq. (36), the equation of S is given by

$$S = \left(I_L + I_0\right) - I_0\left(1 + \frac{qV_{PV}}{\gamma.K.T_c}\right).\left[exp(\frac{dV_{PV}}{\gamma.K.T_c})\right] \tag{48}$$

$$\frac{dS}{dt} = \frac{dS}{dV_{PV}}.\frac{dV_{PV}}{dt} = -I_0\left(\frac{2q}{\gamma.K.T_c} + \frac{qV_{PV}}{\gamma.K.T_c}\right).\left[exp(\frac{dV_{PV}}{\gamma.K.T_c})\right].\frac{\mathrm{dV_{PV}}}{\mathrm{dt}} \tag{49}$$

The stability of the system is summarized in the Table 1.

Table 1 Verification of stability conditions

Variation of S and VPV	S	$\frac{dS}{dV_{\mathrm{PV}}}$
$\frac{dV_{\mathrm{PV}}}{dt} < 0$	Negative	Positive
$\frac{dV_{\mathrm{PV}}}{dt} > 0$	Positive	Negative
$S.\frac{dS}{dt}$	Negative stable system	Negative stable system

8. Simulation Results and Discussion

This section presents the different results of the *SM* optimization of the three investigated *PV* pumping systems. Variable solar radiations were applied to each system, spread over three-time intervals as follows:

(1) From 0 to 3 second, the solar radiation is 1000 W/m^2.

(2) From 3 to 6 second, the solar radiation is 300 W/m^2.

(3) From 6 to 10 second, the solar radiation is 500 W/m^2.

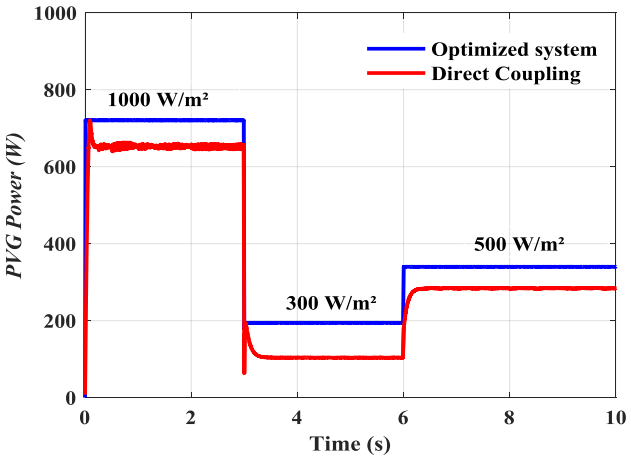

Fig. 9 Power generator of the optimized and direct coupling system

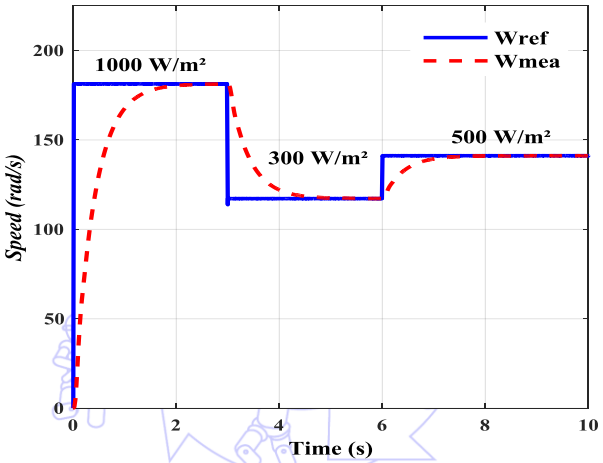

(a) Speed

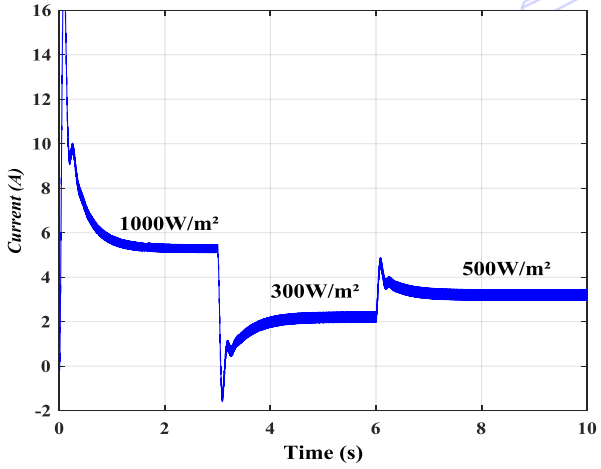

(b) Stator current

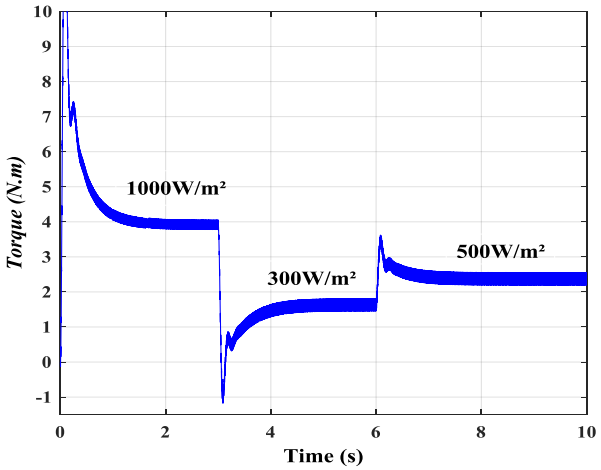

(c) Torque

Fig. 10 Evolution results of the DCM-driven system

Compared with direct coupling, optimization increased the power by approximately 10%, thereby forcing the PVG to operate at its MPP (Fig.9). Fig. 10 illustrates the waveform of the armature current, torque motor, and rotor speed response of the DCM-driven system at variable solar radiation and a fixed temperature (25℃). The depicted inferences prove the feasibility of the proposed control.

For the first time interval with solar radiation of 1000 W/m^2, no difference can be observed between the measured quantities and nominal values; the speed was 183 rad/s with an armature current of 5A. For the second interval, when solar radiation was decreased to 300 W/m^2 (exemplifying situations, such as passing clouds), the new speed was117 rad/s, torque was1.6 Nm, and the armature current was 2.2 A. For the final interval, after increasing solar radiation to 500 W/m^2, speed increased up to 141 rad/s and the torque was proportional to the armature current. Thus, even with varying solar radiation, optimization forced the *PVG* to operate at its MPP. In addition, the transitional regime time was larger (0.6 s) than that of the *PV* pumping systems driven by the *PMSM* and *DCM*.

Fig. 11 shows the results of the direct and quadrature currents, torque motor, and rotor speed response of the system driven by the PMSM at variable solar radiation. The change in solar radiation affected the characteristics of the *PMSM*, and consequently the pump performance. The speed was optimum irrespective of the variations in solar radiation. Furthermore, the direct stator and quadrature currents converged toward their optimal values, i_d =0 A and i_q=6 A, and the torque was proportional to the quadrature current. These results show clearly the effectiveness of the MPPT adapter.

For the third system driven by the *ASM* (Fig. 12), the rotor speed converged to its reference value for any variation in solar radiation, thus achieving the desired flow rate. The quadrature rotor flux magnitude was constantly maintained, and it remained at its reference value of 0.8 Web, demonstrating the efficiency of the flow control loop.

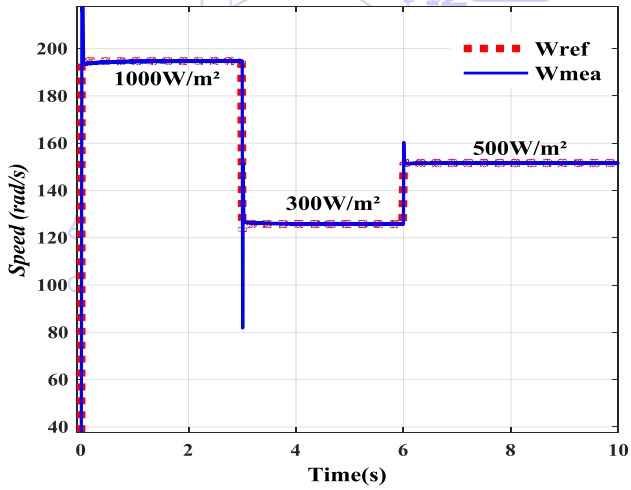

(a) Speed

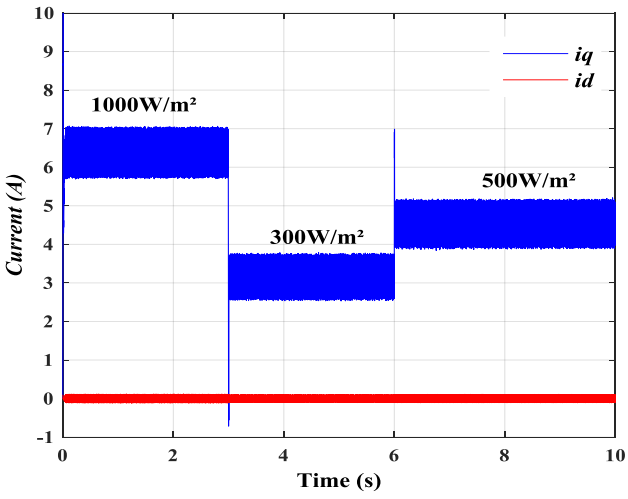

(b) Stator current

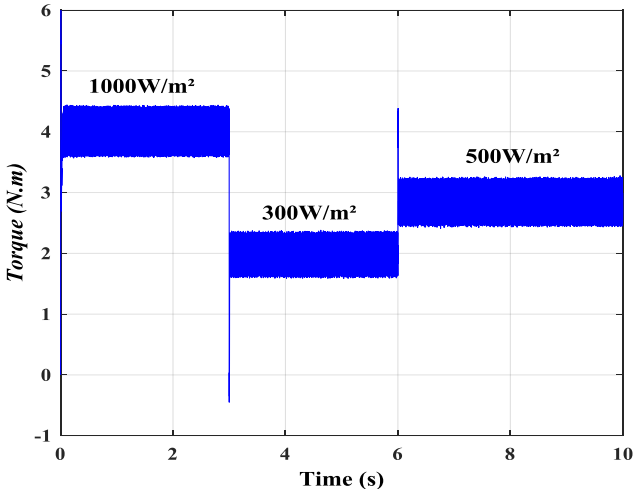

(c) Torque

Fig. 11 Evolution results of the PMSM-driven system

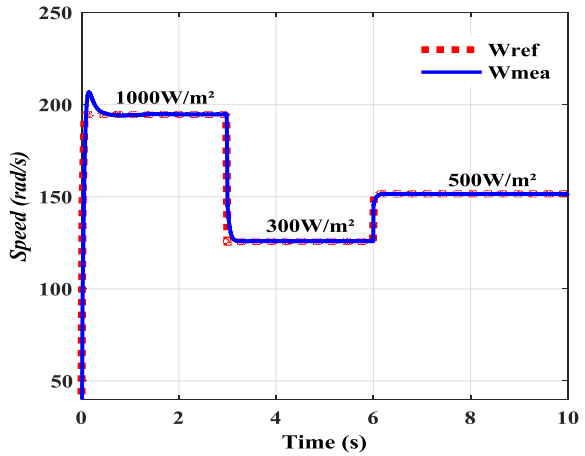

(a) Speed

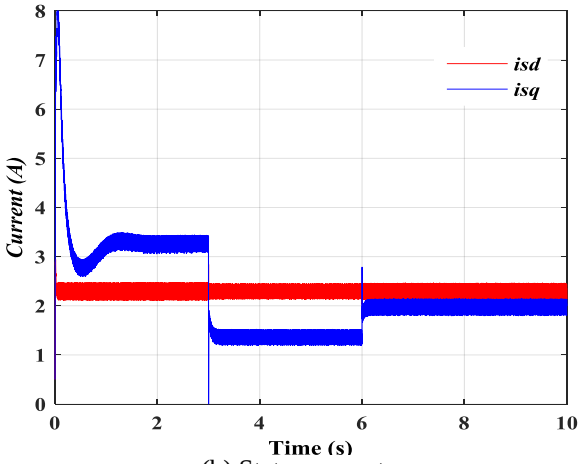

(b) Stator current

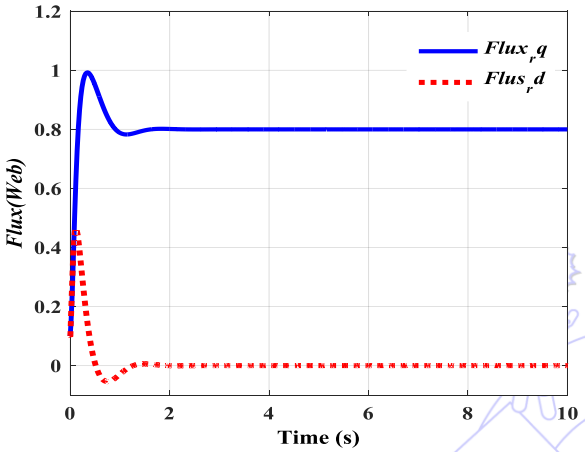

(c) Flux

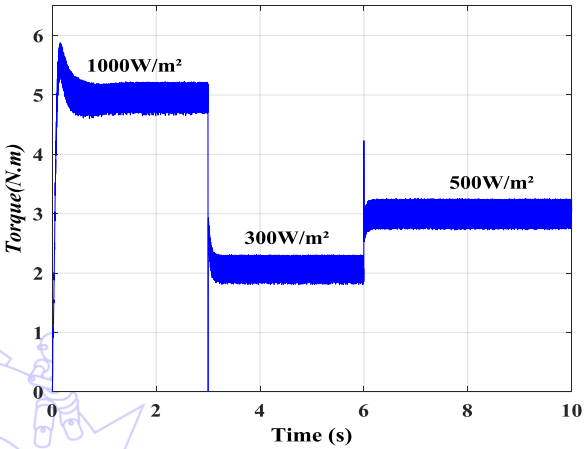

(d) Torque

Fig. 12 Evolution results of the ASM-driven system

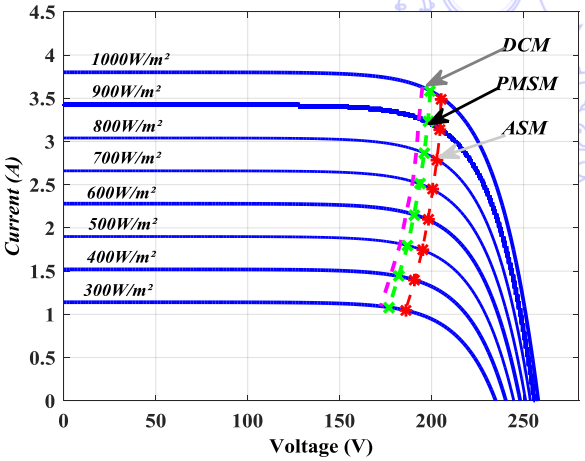

(a) *I* (*V*) characteristics

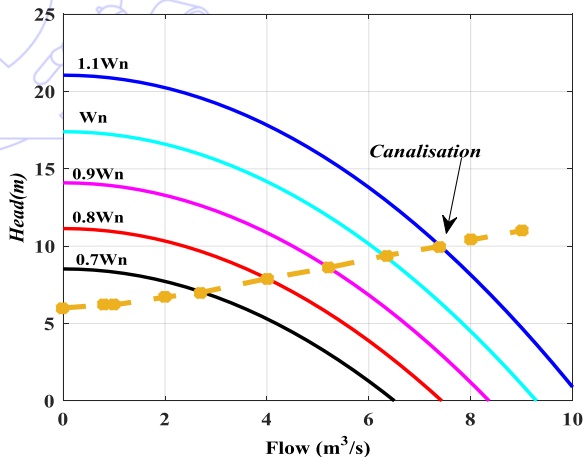

(b) *H* (*Q*) characteristics

Fig. 13 Line of maximum power and *H* (*Q*) characteristics of the pump

The simulation results in optimized and non-optimized cases are illustrated in Figs. 13-15 and Tables 2-4. Optimization with the SM control forced the motor efficiency to function around the MPP; the motor power slipped toward the MPP line of the PVG for illumination varying between 200 and 1000 W/m^2 (Fig. 13(a)).

Fig. 13(b) shows the *H* (*Q*) characteristic; the operating point is the intersection of these two characteristics. Thus, a given speed has only one operating point, which strongly depends on the piping characteristics of the pump. Optimization with the SM forced the pump to supply water at solar radiation of 380, 310, and 260 W/m^2 for the DCM, PMSM, and ASM, respectively, in the optimized systems. By contrast, in the non-optimized systems, this result was obtained at a corresponding solar radiation of 412,365, and 308 W/m^2 (Fig. 14(a)).

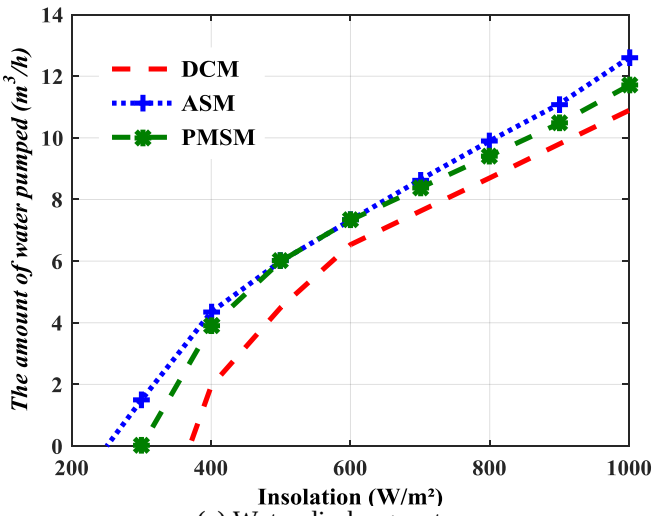

(a) Water discharge rate

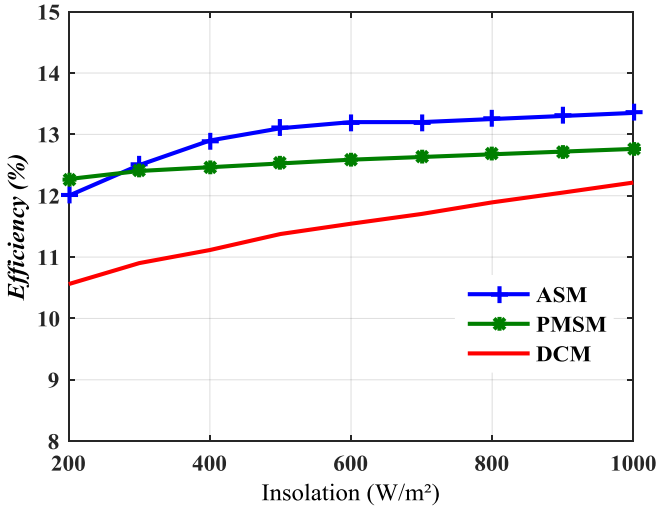

(b) Global efficiencies

Fig. 14 Water discharge rate and the global efficiencies for *DCM*, *PMSM* and *ASM*

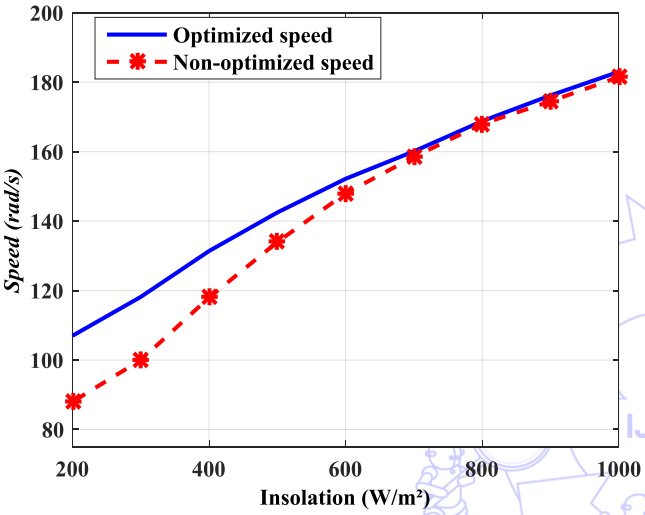

(a) Speed of the *DCM*

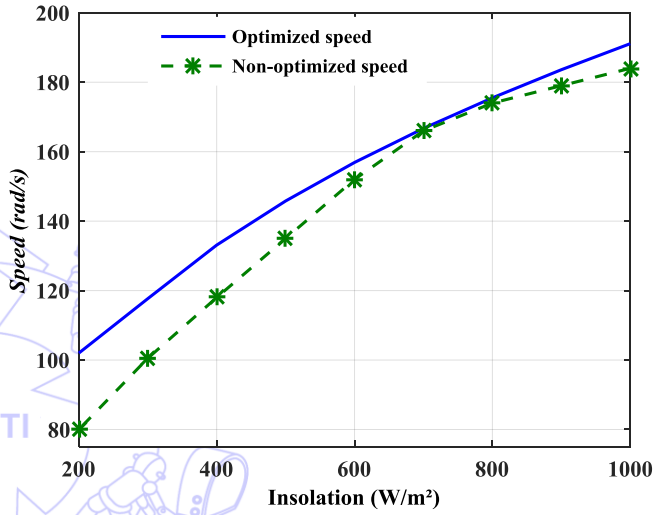

(b) Speed of the *PMSM*

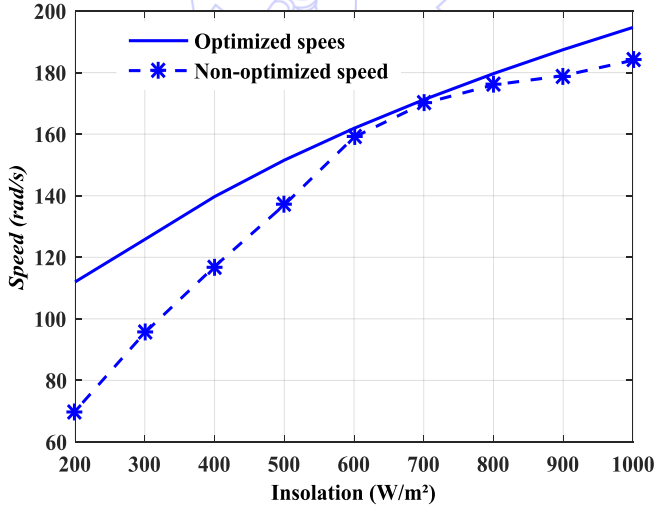

(c) Speed of the *ASM*

Fig. 15 Speed of *PV* pumping systems driven by a *DCM*, *PMSM* and *ASM* for the optimized and non-optimized systems

Tables 2-4 are translations of Figs. 14 and 15, listing the values of the speed, efficiency, and quantity of water pumped per day for direct coupling systems and with *SM* control for each variation in solar radiation. Water discharge for the optimized systems with the *SM* and driven by the *DCM*, *PMSM*, and *ASM* was 86.332, 93.192, and 100.302 m^3/h, respectively, whereas that for the direct coupling systemswas77.986, 78.163, and 84.053 m^3/h, respectively.

Table 2 *PV* water pumping system driven by the *DCM*, with and without optimization

Insolation [W/m^2]	Speed [rad/s]		Efficiency [%]	Water discharge [m^3/h]	
	Non-optimized	optimized		Non-optimized	Optimized
1000	182.321	182.239	12.235	11.015	11.026
900	177.562	178.152	12.023	10.398	10.453
800	168.484	168.484	11.994	8.950	8.950
700	159.913	160.032	11.783	7.821	7.872
600	149.880	152.015	11.642	6.493	6.561
500	132.691	141.563	11.451	3.810	5.109
400	119.325	132.752	11.103	00.985	2.013
300	101.013	119.925	10.918	00.000	00.000
200	89.369	108.482	10.523	00.000	00.000
Amount of water pumped per day [m^3]				77.986	86.332

Table 3 *PV* water pumping system driven by the *PMSM*, with and without optimization

Insolation [W/m^2]	Speed [rad/s]		Efficiency [%]	Water discharge [m^3/h]	
	Non-optimized	optimized		Non-optimized	optimized
1000	184.234	192.145	12.854	11.040	11.902
900	179.910	184.324	12.792	10.982	11.015
800	178.658	178.658	12.779	9.842	9.842
700	169.327	169.857	12.753	8.361	8.395
600	155.321	158.025	12.707	7.346	7.423
500	138.912	144.236	12.619	4.726	6.029
400	119.145	136.589	12.562	2.365	3.991
300	100.058	119.923	12.498	1.058	1.157
200	80.012	102.691	12.326	00.000	00.000
Amount of water pumped per day [m^3]				78.163	93.192

Table 4 *PV* water pumping system driven by the *IM*, with and without optimization

Insolation [W/m^2]	Speed [rad/s]		Efficiency [%]	Water discharge [m^3/h]	
	Non-optimized	optimized		Non-optimized	optimized
1000	182.365	193.026	13.214	11.872	12.810
900	179.895	190.120	13.152	10.960	11.351
800	178.885	180.983	13.129	10.001	10.025
700	175.012	175.058	13.115	8.321	8.410
600	161.105	162.698	13.085	7.390	7.423
500	138.961	153.698	13.046	3.995	6.029
400	119.120	141.023	12.926	2.912	4.281
300	97.752	129.658	12.752	1.123	1.846
200	71.251	116.478	12.045	00.000	00.000
Amount of water pumped per day [m^3]				84.053	100.302

Fig. 14(b) shows that the ASM-driven system had the highest overall efficiency. Accordingly, the amount of water pumped per day by the ASM-driven system (100.302 m^3) was considerably higher than those pumped by the systems driven by the separately excited *DCM* (86.332 m^3) and *PMSM* (93.192 m^3). It can clearly be seen that, the optimization with *SM* improved the efficiency, speed, and quantity of water pumped. Comparison of the performance of the three optimized systems with the direct coupling systems revealed that the *PV* pumping systems driven by the *PMSM* and *ASM* are the most preferred choice for solar-powered water pumping systems.

9. Conclusion

This article compared a three *PV* water pumping systems driven by the *DCM*, *PMSM*, and *ASM* coupled to a centrifugal pump in terms of the global efficiency and water quantity pumped per day. The *SM* control was used to optimize the motor efficiencies and maximize the power delivered by the *PVG* according to the variations in solar radiation at every operation point.

Accordingly, a control based on the choice of a switching function, improved by the addition of an integral error, was used. Compared with the previously reported techniques, the SM control exhibited robustness, accuracy, highest performance, high precision, high stability, and simplicity.

The *PV* pumping system was controlled by a vectorial command in the reference (*dq*).This method helped in providing a satisfactory transient and steady-state performance. In conclusion, the proposed controller is considered as efficient since it fulfills the desired objectives. Furthermore, the *ASM* is the most preferred choice for the present *PV* water pumping system in terms of efficiency and productivity in the steady-state operation owing to the cost-effectiveness and the low maintenance.

References

[1] R. J. Mukti and A. Islam, "Designing an efficient photovoltaic system with maximum power point tracking technique by comparing different converter topologies," Proc. IEEE. 17th International Conf. Computer and Information Technology (ICCIT), IEEE Press, December 2014, pp. 235-240.

[2] A. Chihi, A. Chbeb, and A. Sellami, "Switching function optimization of sliding mode control to a photovoltaic pumping system," Studies in Computational Intelligence, vol. 576, pp. 463-493, November 2014.

[3] M. S. Petibon, "Nouvelles architectures distribuées de gestion et de conversion de l'énergie pour les applications photovoltaïques," Doctoral thesis, Lab. Analysis and architecture of Systems (L.A.A.S), Toulouse Univ, January 2009. (in French).

[4] A. Bouchakour and M. Brahami, "Comparative study between sliding mode control and incremental conductance algorithm to maximize power for photovoltaic systems," European Conference on Renewable Energy Systems (ECRES), Kemer, Antalya, Turkey, October 2015.

[5] A. Betka and A. Attali, "Optimization of a photovoltaic pumping system based on the optimal control theory," Solar Energy, vol. 84, no. 7, pp.1273-1283, April 2010.

[6] H. Abouobaida and M. Cherkaoui, "Comparative study of maximum power point trackers for fast changing environmental conditions," 2012 International Conf. Multimedia Computing and Systems (ICMCS), IEEE Press, May 2012, pp. 1131-1136.

[7] K. Benlarbi and L. Mokrani, "A fuzzy global efficiency optimization of a photovoltaic water pumping system," Solar Energy, vol. 77, no. 2, pp. 203-216, June 2004.

[8] H. Bouzeria, C. Fetha and T. Bahi, "Fuzzy logic space vector direct torque control of PMSM for photovoltaic water pumping system," Energy Procedia, vol. 74, pp. 760-771, April 2015.

[9] M. Akbaba, "Matching induction motors to PVG for maximum power transfer," Desalination, vol. 209, no. 1-3, pp. 31-38, December 2007.

[10] V. C. Mummadi, "Steady-state and dynamic performance analysis of PV supplied DC motors fed from intermediate power converter," Solar Energy Materials & Solar Cells, vol. 61, no. 4, pp. 365-381, February 2000.

[11] J. Appelbaum, "Starting and steady-state characteristics of dc motors powered by solar cell generators," IEEE Transactions on Energy Conversion, vol. EC-1, no. 1, pp. 17-25, March 1986.

[12] K. Benlarbi, "Fuzzy, neuronal and neuro-fuzzy optimization of a photovoltaic water pumping system driven by DC an AC motors," Master Thesis, Dept. Elect, Batna Univ., Algeria 2003. (in French)

[13] P. Packiam and N. K. Jain, "Steady and transient characteristics of a single stage PV water pumping system," Energy Systems, vol. 6, no. 2, pp. 173-199, December 2014.

[14] A. Bouchakour and M. Brahami, "A comparative and analytical study of various MPPT techniques applied in PV systems for fast changing environmental conditions," 3rd International Renewable and Sustainable Energy Conference, December 2015.

[15] M. Di Piazza and G.P. Vitale, "Photovoltaic sources, modeling and emulation," London: Springer- Verlag London, Chapter 4, p. 84, 2013.

[16] A. Bouchakour and M. Brahami, "Study of a photovoltaic system using MPPT Buck-Boost converter," International Journal of Materials, Mechanics and Manufacturing, vol. 3, no. 1, pp. 65-68, February 2015.

[17] M. Rabia Benayeche, "Contribution à la commande robuste des systèmes non linéaires incertains : application à un système hydraulique," Doctoral thesis, Lab. Innovates. Tech. (L.I.T), Valenciennes Univ., December 2009. (in French)

[18] M. Arrouf and S. Ghabrour, "Modeling and simulation of a pumping system fed by photovoltaic generator within the Simulink programming environment," Desalination Solar Energy, vol. 209, no. 1, pp. 23-30, April 2007.

[19] H. S. Ramirez and R. S. Ortigoza, "Control design techniques in power electronics devices," London: Springer- Verlag London, pp. 235-358, 2006.

[20] A. Mokeddem and A. Midoun, "Performance of a directly-coupled PV water pumping system," Energy Conversion and Management, vol. 52, no. 10, pp. 3089-3095, April 2011.
[21] O. Atlam and M. Kolhe, "Performance evaluation of directly photovoltaic powered DC PM (direct current permanent magnet) motor-propeller thrust system," Energy, vol. 57, pp. 692-698, June 2013.
[22] L. Zarour, R. Chenni, "Improvement of synchronous and asynchronous motor drive systems supplied by photovoltaic arrays with frequency control," Journal of Electrical Engineering, vol. 59, no. 4, pp. 169-177, 2008.
[23] A. Khalief, "Contribution à la commande vectorielle sans capteur mécanique des machines synchrones à aimant permanents (MSAP), " Doctoral thesis, Dept. Elect. Eng., Marseille Univ., 2012. (in French)
[24] A. Ghoneim, "Design optimization of photovoltaic powered water pumping systems," Energy Conversion and Management, vol. 47, no. 11, pp. 1449-1463, October 2006.
[25] J. P. Carou and J. P. Hautier, "Modélisation et commande de la machine asynchrone," Méthode et pratique de l'ingénieur, Paris, Chapter 2, p. 42,1995. (in French)
[26] S. R. Wenham, M. A. Green, M. E. Watt, and R. Corkish, Applied photovoltaics, 2nd ed., London: Earthscan, Chapter 11, p. 222, 2007.
[27] A. Borni, "Etude et optimisation d'un multi système hybride de conversion d'énergie électrique," Doctoral thesis, Dept. Elec. Eng Sciences., Constantine 1 Univ., 2015. (in French)

Appendix

Photovoltaic module parameters (G =1000 W/m², T =25 ° C) [27]:

P_n= 60 W, I_{sc}=3.7A, I_{op}=3.5 A, V_{oc}=22.5 V, V_{op}=17.3 V, Rs= 0.08 Ω, Np=1, Ns=12.

DC motor parameters [8, 23]:

P_n=746 W, e_a=180 V, ia=5.5 A, R_a=8.03 Ω, L_a=0.045 H, K_E=0.741 V/(rad/s), P=2, J_m=0.024 Kg/m^2, B_m=0 Nm/(rad/s), K_T=0.741 Nm/A.

PMS motor parameters [8]:

P_n=746 W, I_{sn}=6 A, R_s=1.93 Ω, R_r=1.143 Ω, L_d=0.0424 H, L_q=0.00795 H, P=2, J_m= 0.003 Kg/m^2, B_m= 8e^{-4} Nm/(rad/s).

AS motor parameters [8]:

P_n= 746 W, I_{sn}= 3.4 A, R_s= 4 Ω, R_r= 1.143 Ω, L_s= 0.3676 H, L_r=0.3676 H, M=0.3489 H, P=2, J_m=0.003 Kg/m^2, B_m=98e^{-4} Nm/(rad/s).

Centrifugal pump parameters [8]:

P_n=560 W, a_0=4.9234e^{-3} m/(rad/s)^2, a_1=1.5825e^{-5} m/(rad/s) (m^2/s), a_2=-18144 m/(m^3/s)^2.

Canalization parameters:

H_g=10 m, l=7.4 m, λ=0.0396 m, d=0.06 m, g=9.81 m^2/s.